


Few-Femtosecond MeV Electron Bunches for Ultrafast Electron Diffraction

Cheng Li¹, Wenxing Wang¹, Haoran Zhang¹, Zixin Guo, Xiazhen Xu, Zhigang He^{1,*},
Shancai Zhang, Qika Jia, Lin Wang, and Duohui He

*National Synchrotron Radiation Laboratory, University of Science and Technology of China, Hefei,
Anhui 230029, China*

 (Received 3 January 2022; revised 9 March 2022; accepted 2 May 2022; published 6 June 2022)

Herein, we propose a technique for megaelectronvolt ultrafast electron diffraction that can achieve a few-femtosecond time resolution. The technique modulates a relativistic electron beam using two radially polarized laser pulses of varying frequencies, which enable the condensation of the electrons into an ultrashort pulse. Moreover, our study shows that this technique can suppress the arrival-time jitter of the electron beam at the sample location. Numerical simulations show that using realistic laser parameters corresponding to the current gigawatt-power-level laser systems, a 3.3-fs (rms over 45% charge) electron beam can be obtained and the arrival-time jitter can be 1.35 fs (rms). This technique may have a considerable impact on ultrafast electron diffraction, microscopy, and other ultrafast research facilities that require few-femtosecond electron beams with a small time jitter.

DOI: [10.1103/PhysRevApplied.17.064012](https://doi.org/10.1103/PhysRevApplied.17.064012)

I. INTRODUCTION

Ultrafast electron diffraction (UED) with femtosecond temporal resolution and angstrom spatial resolution is an important tool for understanding the structural transitions in biology, chemistry, material science, etc. [1–9].

Most UED facilities normally employ photocathode high-voltage guns to generate and accelerate electron beams to an energy range of tens to hundreds of kiloelectronvolts [10–12]. Due to the space-charge effect and the temporal dispersion during the dc acceleration, the electron beam will be broadened, which limits the time resolution. Many methods have been proposed to compress electron beams at the kiloelectronvolt energy level [13,14]. However, in order to achieve a high time resolution, the electron beam can only contain hundreds of electrons at the most.

With a given amount of electron charge, a shorter electron pulse duration is achievable with relativistic electron beams at the megaelectronvolt energy level compared to nonrelativistic electron beams at lower energies [15,16]. Furthermore, a megaelectronvolt UED based on a photocathode rf gun is widely used in pump-probe experiments, taking advantage of the fact that the drive pulse is tightly synchronized with the pump pulse. Several studies have been done to achieve single-shot megaelectronvolt UED based on a photocathode rf gun [17–21]. The time resolution is mainly limited by the pulse duration and time jitter of the electron beam. Therefore, one of the long-term goals

is to produce ultrashort electron beams with a small time jitter.

In recent years, many methods have been studied to improve the time resolution of megaelectronvolt UED based on a photocathode rf gun [22–31]. Two optical fields at different frequencies in vacuum are used to form a ponderomotive force in the direction of electron propagation and the propagation velocity of the traveling wave is synchronized to the electron velocity, leading to a compression of the electron beam and the formation of an ultrashort pulse. To match the velocity of relativistic electron beams, the two laser pulses need to be incident at a small angle, which is difficult to achieve [22,23]. Megaelectronvolt electron beams can be compressed to 10 fs (rms) by using a rf buncher; however, the arrival-time jitter of the compressed bunch increases to above 100 fs [24,25]. With the Coulomb force from the front and back drive electron beams, the target beam at the central position has been compressed to less than 50 fs [26]. The electron beam can be compressed to subfemtoseconds by the field of a synchronized radially polarized laser (RPL) pulse that is focused near the cathode surface [27]. In the scheme, the electron beam is modulated at a low energy (kiloelectronvolts) and then the modulated electron beam is accelerated to several megaelectronvolts by the rf field in the gun cavity. Since the electron beam interacts with the laser at a low energy (kiloelectronvolts), the capacity of the bunch charge is low. By replacing the aforementioned rf buncher with a terahertz-driven buncher, megaelectronvolt electron beams can be compressed to about 30 fs (rms) and the arrival-time jitter can be reduced to about 30 fs

*hezhg@ustc.edu.cn

[28,29]. With a double-bend achromat compressor, 20-fs mega-electronvolt electron beams have been obtained and the arrival-time jitter is below 20 fs [30,31]. Although there are many advances in mega-electronvolt UED, the generation of few-femtosecond high-charge electron beams with a few-femtosecond time jitter still remains a challenge.

II. PRINCIPLE

In this paper, we identify a regime to compress a relativistic electron beam by using the longitudinal-electric-field components of two-color RPL pulses (a linearly polarized infrared laser can be converted into a RPL pulse by a commercial vortex wave plate and the transmission efficiency can reach 99%). The schematic layout is shown in Fig. 1(a). An electron beam is emitted from the photocathode under the illumination of a third-harmonic drive-laser pulse (266.7 nm) and accelerated rapidly to several mega-electronvolts by the rf field in the gun cavity. Then, the relativistic electron beam interacts with two RPL pulses (focused by an OAP mirror) of different frequencies near the focal position. The time interval corresponding to the frequency difference of the two-color RPL pulses is approximately equal to the duration of the electron beam;

thus most of the electrons can be bunched into an ultrashort density peak after two-color energy modulation and a free-space drift. The frequency difference of the two RPL pulses can be adjusted to compress electron beams with different pulse durations. In addition, this scheme can suppress the arrival-time jitter caused by the phase and amplitude jitter of the rf field in a photocathode rf gun. For instance, our numerical demonstration shows that a 140-fs electron beam of 8.0 fC charge can be compressed to a 3.3-fs (rms) spike that contains 3.6 fC charge and the arrival-time jitter can be reduced from 9.8 fs (rms) to 1.35 fs (rms).

The physics behind this scheme is illustrated in this section. Direct acceleration of electrons in an infinite vacuum by focused RPL pulses with terawatt- (TW) level peak power is particularly attractive [32–37]. Electrons are accelerated by the strong longitudinal-electric-field component, while the radial field components confine the electrons close to the optical axis. The main difficulty of accelerating electrons in vacuum is that the phase velocity of the laser pulse is higher than the velocity of the electrons, which leads to a phase slippage between the electrons and the laser pulse. Thus, the electrons pass through the periodic acceleration phase and deceleration phase of the laser field and cannot gain net energy from a plane

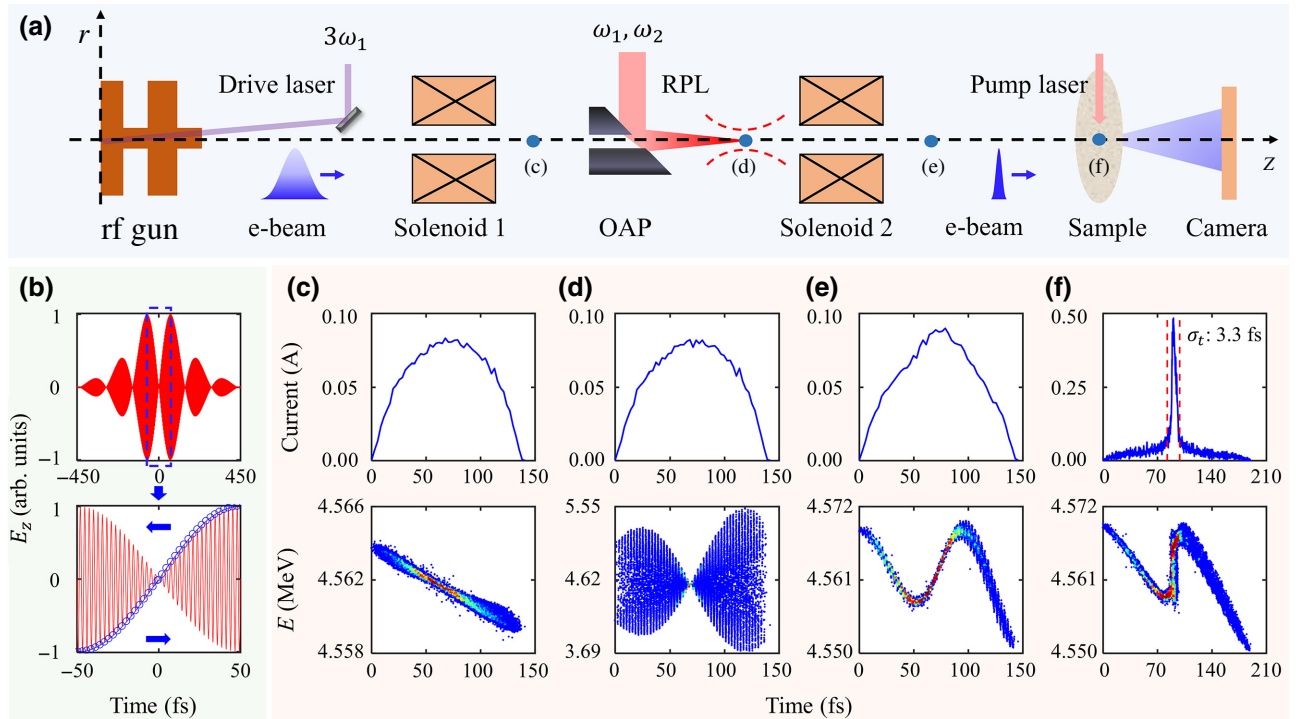


FIG. 1. (a) The schematic layout. (b) The longitudinal-field-superposition diagram of two-color RPL pulses: the blue circles represent the electrons that drift to form density modulation and the blue arrows indicate the drift trajectories. (c)–(f) The longitudinal phase space and the current distribution of the electron beam, (c) before modulation at 0.5 m downstream of the photocathode surface, (d) at the focus location, which is 0.535 m downstream of the photocathode surface, (e) after modulation at 0.57 m downstream of the photocathode surface, and (f) at the sample location, which is 0.951 m downstream of the photocathode surface. OAP, off-axis parabolic, which is used to focus the RPL. Solenoids 1 and 2 are used to focus the electron beam and the camera is used to measure the diffraction pattern.

wave or a pulse wave. For the focused RPL pulse, the field amplitude of the laser pulse increases when it approaches the focal plane and then decreases as it leaves the focal plane. The relativistic electrons, the velocity of which is close to the velocity of light, interact with the laser pulse, making it stay in the acceleration half cycle for a long time. When the electrons enter the deceleration half cycle, the field amplitude of the laser, which is inversely proportional to the square of the spot radius, is weakened by the diffraction effect. For example, to make a simple estimate, using the parameters listed in Table I and ignoring the change of laser phase velocity, the time of the electron beam slipping a half phase cycle is $\lambda/2(1 - \beta)c = 0.262$ ps, where λ is the laser wavelength, β is the normalized electron velocity, and c is the speed of light. After this time interval, the field amplitude of the laser can be reduced by a half. The electrons will experience a few asymmetric acceleration and deceleration cycles until the laser axial field disappears. In this way, a net energy gain can be obtained by the electrons. In this paper, two-color RPL pulses with gigawatt- (GW) level peak power are used to modulate rather than accelerate a relativistic electron beam. First, we ignore the influence of the phase-slippage effect. In this case, it is similar to the modulation of the electron beam in the vicinity of a nanostructure that is excited by incident light fields with two frequencies [38]. In the slowly varying envelope approximation, the energy modulation obtained by the electron beam near the laser focus can be written as $\Delta E(t) = E_0(t) \cos(\omega t - \phi)$, where $E_0(t)$ is the temporal envelope of the energy-modulation amplitude of the electrons, ω is the laser angular frequency, and ϕ is the phase of the energy modulation. Using two-color RPL pulses, the energy modulation becomes $\Delta E(t) = E_{01}(t) \cos(\omega_1 t - \phi_1) + E_{02}(t) \cos(\omega_2 t - \phi_2)$. Assuming that the two-color RPL pulses have the same temporal envelope and that $\phi_1 = -\phi_2 = \pi/2$, the energy modulation can be simplified as $\Delta E(t) = 2E_0(t) \sin((\omega_1 - \omega_2)/2)t \cos((\omega_1 + \omega_2)/2)t$, where the first term is the slowly varying part and the last term is the rapidly oscillating part. After the energy modulation, by setting an appropriate drift distance, the electrons represented by the blue circles in Fig. 1(b) can be compressed into a few femtoseconds, as indicated by the blue arrows in Fig. 1(b). However, due to the phase-slippage effect, the real situation is more complicated. At the laser-focus location, the two-color RPL pulses catch up and modulate the electron beam in Fig. 1(c). The real longitudinal phase space of the electron beam obtained by simulation at the laser-focus location can be seen in Fig. 1(d). When passing through the focal location, the electron beam continues to interact with the two-color RPL pulses. The center of the electron beam has a slippage relative to the two-color RPL-pulse node. In the meantime, the modulation amplitude of the electron beam will decrease until the axial field of the laser disappears. As mentioned above, as the size of the laser grows larger,

the axial field becomes weaker and the energy modulation shown in Fig. 1(d) cannot be canceled out. Consequently, the longitudinal phase space of the electron beam is shown in Fig. 1(e). After passing through a free-space drift, the energy modulation is converted into density modulation at the sample location, as shown in Fig. 1(f). Due to the phase-slippage effect, more electrons can be captured in the density peak.

III. SIMULATION

In the following, we demonstrate the proposed scheme by using a three-dimensional relativistic particle-tracing simulation with the GENERAL PARTICLE TRACER code [39]. The derivation of the RPL fields can be found in Ref. [27,34]. The space-charge effect is included and 50 000 macroparticles (one macroparticle for one real electron) are used in the simulation. The main parameters are summarized in Table I.

As shown in Fig. 1(c), due to the space-charge effect, an initial 50-fs electron beam with uniform temporal distribution is broadened to more than 100 fs. The initial electron beam can be replaced by a Gaussian distribution with a full width at half maximum (FWHM) of 50 fs, which will not affect the simulation results. Then, the electron beam experiences the optical fields of the two-color RPL pulses at wavelengths of 800 nm and 821.9 nm. The time interval corresponding to the frequency difference of the two-color RPL pulses is 100 fs. The duration of the two RPL pulses is 0.2 ps, which needs to be greater than the time interval corresponding to the frequency difference of the two-color RPL pulses. For a given laser-pulse duration, beam waist radius, and sample location, a laser energy of 1.4 mJ is

TABLE I. The main parameters.

Parameters	Values
<i>Parameters of the gun</i>	
Electric field amplitude E_{01}	95 MV/m
Frequency	2856 MHz
Launch phase ψ	298°
Output energy	4.561 MeV
<i>Initial electron-beam parameters</i>	
Beam charge	8 fC
Number of electrons	50 000
Radius (uniform)	30 μm
Initial pulse duration (uniform)	50 fs
Thermal emittance	10.8 nm rad
<i>Solenoid parameters</i>	
Solenoid strength	0.31 T
Effective length	0.2 m
<i>Two-color RPL-pulse parameters</i>	
Pulse duration (Gaussian, FWHM)	0.2 ps
Radius at the focus location	5 μm
Wavelength	800 nm/821.9 nm
Pulse energy	1.4 mJ

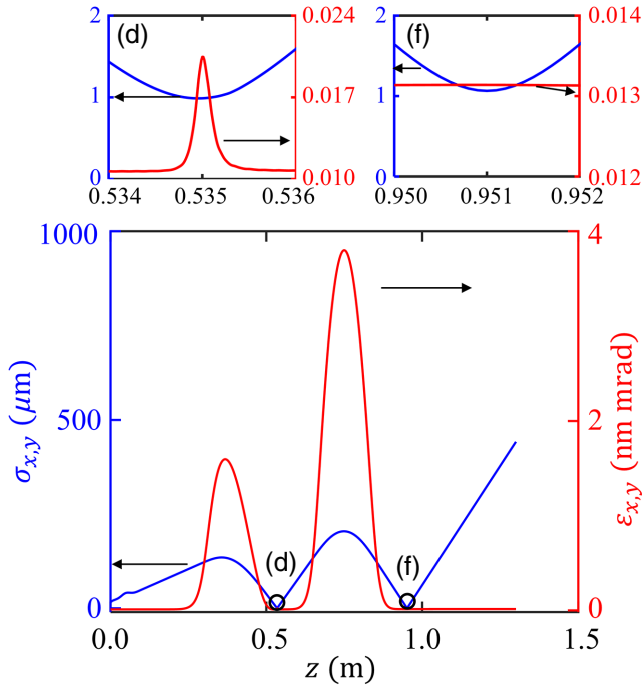


FIG. 2. The transverse beam size and the transverse normalized emittance from the photocathode ($z = 0$ m) to the sample location ($z = 0.951$ m). Enlargements of positions (d) and (f) (see Fig. 1) are shown in the upper plots.

selected based on the simulation results. In addition, for a 1% laser energy jitter, there is almost no effect on the compressed bunch length and the time for the electron beam to reach the sample location. As shown in Fig. 1(f), at the sample location, the electron beam is compressed to 3.3 fs (rms), which is the rms width of the electron beam in the time window indicated by two dashed red lines corresponding to the peak current dropping to 15%. The ratio of electrons captured in the time window is about 45% and the charge is approximately 3.6 fC. Meanwhile, to confine the transverse beam size at the laser focus and sample location, two solenoid fields are added in the simulation. Additionally, the transverse normalized emittance of the electron beam is important for UED, which affects the quality of the diffraction patterns [40]. As shown in Fig. 2, the transverse beam size at the laser focus and sample location is about $1 \mu\text{m}$ (rms) and the transverse normalized emittance at the sample location is 13.1 nm rad, which is close to the initial thermal emittance. At the range of ± 1 mm from the sample position, the duration of the electron beam and the transverse normalized emittance is constant and the transverse beam size is less than $2 \mu\text{m}$ (rms).

To obtain an electron beam with a larger charge, the frequency difference of the two-color RPL pulses can be reduced; thus the time interval corresponding to the frequency difference will be longer. In this way, the energy modulation obtained by the electron beam is more linear

and more electrons can be captured in the density peak. However, a higher laser energy is needed. As shown in Fig. 3, by reducing the frequency difference of the two-color RPL pulses and increasing the laser energy to 2.8 mJ, the charge of the electron beam in the same time window can be increased from 3.6 fC to 4.85 fC. Furthermore, since the time interval corresponding to the frequency difference increases, a longer electron beam can be compressed.

IV. TEMPORAL RESOLUTION

The time resolution τ is a critical figure of merit. It can be expressed as

$$\tau = \sqrt{\tau_{\text{pump}}^2 + \tau_{\text{probe}}^2 + \tau_{\text{jitter}}^2 + \tau_{\text{VM}}^2}, \quad (1)$$

where τ_{pump} and τ_{probe} are the pulse duration of the pump-laser pulse and the probe-electron pulse, respectively. τ_{jitter} is the arrival-time jitter between the pump-laser pulse and the probe-electron pulse at the sample location and τ_{VM} is the velocity mismatch term. The rms pulse width τ_{pump} of the pump laser can reach a few femtoseconds or even the subfemtosecond range. For micrometer or thinner samples, τ_{VM} is negligible. To achieve a high time resolution, it is necessary to reduce the arrival-time jitter.

For the photocathode rf gun, the phase and amplitude jitter of the rf field will cause an energy fluctuation of the electron beam, which leads to an arrival-time jitter. The scheme we propose can suppress this jitter. Since the two-color RPL pulses and the drive-laser pulse originate from the same laser source, the phase error between them is negligible. The electron beam generated from the photocathode rf gun has an energy chirp, which is caused by the space-charge effect. As shown in Fig. 1(c), the energy at

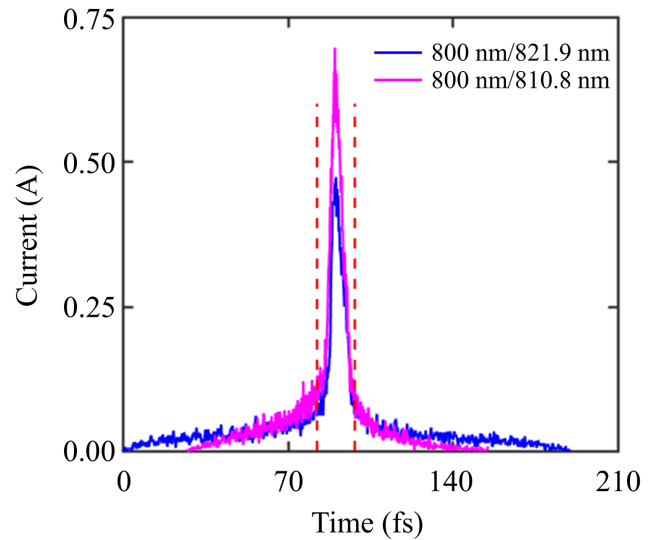


FIG. 3. The current distribution of the electron beam at the sample location.

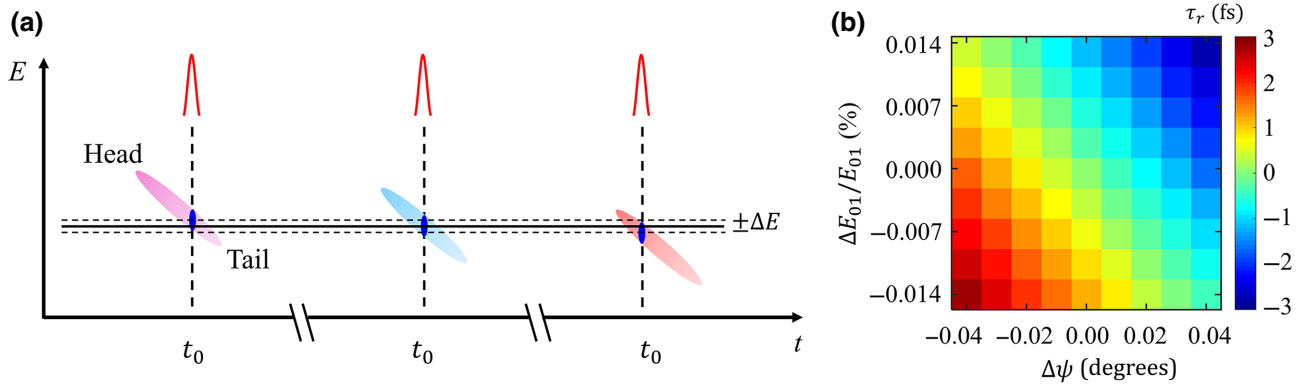


FIG. 4. (a) The schematic diagram of jitter analysis. (b) The simulation result of the relative arrival time (τ_r) at the sample location as influenced by the rf phase (ψ) and the rf electric-field-amplitude (E_{01}) fluctuation. t_0 is the time for the ideal electron beam to reach the focal position.

the head of the electron beam is higher than that at the tail. For an ideal situation, the center of the electron beam will be modulated by the two-color RPL pulses, as shown in the middle diagram of Fig. 4(a). When the energy of the electron beam increases due to the rf amplitude or phase jitter, the tail of the electron beam meets the two RPL pulses and this part of the electron beam, the energy of which is lower than that of electrons at the center, as shown in the left diagram of Fig. 4(a). Based on the same principle as above, when the energy of the electron beam decreases, the head of the electron beam, the energy of which is higher than that of electrons at the center, is modulated, as shown in the right diagram of Fig. 4(a). The energy difference of the electrons in the modulated parts can be very small in these three situations. It can be predicted that this scheme can effectively suppress the time jitter. Figure 4(b) shows the simulation results of the relative arrival time at the sample location as influenced by the rf phase and amplitude fluctuation. With the state-of-the-art technology achieved in SwissFEL [41], the synchronization between the laser and the rf signal can be controlled below 20 fs (rms), which corresponds to 0.02° phase jitter for a rf of 2856 MHz and a rf power fluctuation of 1.3×10^{-4} (rms), which is twice the electric-field-amplitude fluctuation. By adopting the above technologies, the arrival-time jitter can be kept at about 1.35 fs (rms).

In addition, to generate a subfemtosecond electron pulse with a subfemtosecond time jitter, we can reduce the length of the second solenoid and increase the magnetic field strength to make the sample location move closer to the photocathode. For example, the pulse duration of the electron beam can be reduced from 3.3 fs (rms) to 0.94 fs (rms) at 0.73 m away from the cathode surface and the time jitter will be further reduced due to the reduced distance between the modulation location and the sample location. However, compared with the aforementioned solenoids, which are widely used in photocathode rf guns, the solenoids used here may be difficult in technical practice and as the sample

location moves closer to the photocathode, a higher laser energy is required.

V. CONCLUSIONS

In conclusion, we demonstrate a scheme to reduce the pulse duration and time jitter of a relativistic electron beam through beam compression driven by two-color RPL pulses. Simulation results show that a 3.6-fC electron beam with a pulse duration of 3.3 fs (rms) can be generated by using a mature photocathode rf gun and a commercial gigawatt-power-level laser system, while keeping the time jitter at 1.35 fs (rms). The transverse emittance of the electron beam can be close to the initial thermal emittance and the peak current can reach 0.48 A. The frequency difference of the two-color RPL pulses can be tuned to obtain an electron beam with a larger charge. By reducing the distance between the laser focus and the sample and increasing the laser energy, the pulse duration and time jitter of the electron beam can be reduced further. The proposed scheme can be applied to megaelectronvolt UED measurement and can achieve a very good time resolution. We also hope that this scheme can be widely used in many other research fields.

ACKNOWLEDGMENTS

This work is supported by the National Natural Science Foundation of China (Grant No. 11775216) and the Youth Innovation Promotion Association (CAS).

-
- [1] P. Brazda, L. Palatinus, and M. Babor, Electron diffraction determines molecular absolute configuration in a pharmaceutical nanocrystal, *Science* **364**, 667 (2019).
 - [2] T. Frigge, B. Hafke, T. Witte, B. Krenzer, C. Streubuhr, A. S. Syed, V. M. Trontl, I. Avigo, P. Zhou, M. Ligges, D. von der Linde, U. Bovensiepen, M. Horn-von Hoegen,

- S. Wippermann, A. Lucke, U. Gerstmann, and W. G. Schmidt, Optically excited structural transition in atomic wires on surfaces at the quantum limit, *Nature* **544**, 207 (2017).
- [3] C. J. Hensley, J. Yang, and M. Centurion, Imaging of Isolated Molecules with Ultrafast Electron Pulses, *Phys. Rev. Lett.* **109**, 133202 (2012).
- [4] L. Palatinus, P. Brazda, P. Boullay, O. Perez, M. Klementova, S. Petit, V. Eigner, M. Zaarour, and S. Mintova, Hydrogen positions in single nanocrystals revealed by electron diffraction, *Science* **355**, 166 (2017).
- [5] J. Yang *et al.*, Imaging CF₃I conical intersection and photodissociation dynamics with ultrafast electron diffraction, *Science* **361**, 64 (2018).
- [6] M. Z. Mo, Z. Chen, R. K. Li, M. Dunning, B. B. L. Witte, J. K. Baldwin, L. B. Fletcher, J. B. Kim, A. Ng, R. Redmer, A. H. Reid, P. Shekhar, X. Z. Shen, M. Shen, K. Sokolowski-Tinten, Y. Y. Tsui, Y. Q. Wang, Q. Zheng, X. J. Wang, and S. H. Glenzer, Heterogeneous to homogeneous melting transition visualized with ultrafast electron diffraction, *Science* **360**, 1451 (2018).
- [7] E. J. Sie *et al.*, An ultrafast symmetry switch in a Weyl semimetal, *Nature* **565**, 61 (2019).
- [8] J. Yang, X. Zhu, J. P. F. Nunes, J. K. Yu, R. M. Parrish, T. J. A. Wolf, M. Centurion, M. Gühr, R. Li, Y. Liu, B. Moore, M. Niebuhr, S. Park, X. Shen, S. Weathersby, T. Weinacht, T. J. Martinez, and X. Wang, Simultaneous observation of nuclear and electronic dynamics by ultrafast electron diffraction, *Science* **368**, 885 (2020).
- [9] A. A. Ischenko, P. M. Weber, and R. D. Miller, Capturing chemistry in action with electrons: Realization of atomically resolved reaction dynamics, *Chem. Rev.* **117**, 11066 (2017).
- [10] Y. Morimoto and P. Baum, Diffraction and microscopy with attosecond electron pulse trains, *Nat. Phys.* **14**, 252 (2018).
- [11] D. Ehberger, K. J. Mohler, T. Vasileiadis, R. Ernstorfer, L. Waldecker, and P. Baum, Terahertz Compression of Electron Pulses at a Planar Mirror Membrane, *Phys. Rev. Appl.* **11**, 024034 (2019).
- [12] K. J. Mohler, D. Ehberger, I. Gronwald, C. Lange, R. Huber, and P. Baum, Ultrafast electron diffraction from nanophotonic waveforms via dynamical Aharonov-Bohm phases, *Sci. Adv.* **6**, eabc8804 (2020).
- [13] K. E. Priebe, C. Rathje, S. V. Yalunin, T. Hohage, A. Feist, S. Schäfer, and C. Ropers, Attosecond electron pulse trains and quantum state reconstruction in ultrafast transmission electron microscopy, *Nat. Photonics* **11**, 793 (2017).
- [14] Y. Morimoto and P. Baum, Single-Cycle Optical Control of Beam Electrons, *Phys. Rev. Lett.* **125**, 193202 (2020).
- [15] O. Lundh, J. Lim, C. Rechatin, L. Ammoura, A. Ben-Ismaïl, X. Davoine, G. Gallot, J.-P. Goddet, E. Lefebvre, V. Malka *et al.*, Few femtosecond, few kiloampere electron bunch produced by a laser-plasma accelerator, *Nat. Phys.* **7**, 219 (2011).
- [16] C. M. Sears, E. Colby, R. Ischebeck, C. McGuinness, J. Nelson, R. Noble, R. H. Siemann, J. Spencer, D. Walz, T. Plettner *et al.*, Production and characterization of attosecond electron bunch trains, *Phys. Rev. Special Top.—Accel. Beams* **11**, 061301 (2008).
- [17] P. F. Zhu, Y. Zhu, Y. Hidaka, L. Wu, J. Cao, H. Berger, J. Geck, R. Kraus, S. Pjerov, Y. Shen, R. I. Tobey, J. P. Hill, and X. J. Wang, Femtosecond time-resolved MeV electron diffraction, *New J. Phys.* **17**, 063004 (2015).
- [18] F. C. Fu, S. G. Liu, P. F. Zhu, D. Xiang, J. Zhang, and J. M. Cao, High quality single shot ultrafast MeV electron diffraction from a photocathode radio-frequency gun, *Rev. Sci. Instrum.* **85**, 083701 (2014).
- [19] P. Musumeci, J. T. Moody, C. M. Scoby, M. S. Gutierrez, H. A. Bender, and N. S. Wilcox, High quality single shot diffraction patterns using ultrashort megaelectron volt electron beams from a radio frequency photoinjector, *Rev. Sci. Instrum.* **81**, 013306 (2010).
- [20] J. Hastings, F. Rudakov, D. Dowell, J. Schmerge, J. Cardoza, J. Castro, S. Gierman, H. Loos, and P. Weber, Ultrafast time-resolved electron diffraction with megavolt electron beams, *Appl. Phys. Lett.* **89**, 184109 (2006).
- [21] J. Yang, K. Gen, N. Naruse, S. Sakakihara, and Y. Yoshida, A compact ultrafast electron diffractometer with relativistic femtosecond electron pulses, *Quantum Beam Sci.* **4**, 4 (2020).
- [22] M. Kozak, N. Schonenberger, and P. Hommelhoff, Ponderomotive Generation and Detection of Attosecond Free-Electron Pulse Trains, *Phys. Rev. Lett.* **120**, 103203 (2018).
- [23] M. Kozak, T. Eckstein, N. Schonenberger, and P. Hommelhoff, Inelastic ponderomotive scattering of electrons at a high-intensity optical travelling wave in vacuum, *Nat. Phys.* **14**, 121 (2018).
- [24] J. Maxson, D. Cesar, G. Calmasini, A. Ody, P. Musumeci, and D. Alesini, Direct Measurement of Sub-10 fs Relativistic Electron Beams with Ultralow Emittance, *Phys. Rev. Lett.* **118**, 154802 (2017).
- [25] L. R. Zhao *et al.*, Terahertz Streaking of Few-Femtosecond Relativistic Electron Beams, *Phys. Rev. X* **8**, 021061 (2018).
- [26] C. Lu, T. Jiang, S. G. Liu, R. Wang, L. R. Zhao, P. F. Zhu, D. Xiang, and J. Zhang, Coulomb-Driven Relativistic Electron Beam Compression, *Phys. Rev. Lett.* **120**, 044801 (2018).
- [27] C. Li, W. X. Wang, H. R. Zhang, Z. X. Guo, S. M. Jiang, Z. G. He, S. C. Zhang, Q. K. Jia, L. Wang, and D. H. He, Relativistic Attosecond Electron Pulses from a Photocathode Radio-Frequency Gun, *Phys. Rev. Appl.* **16**, 054007 (2021).
- [28] E. C. Snively, M. A. K. Othman, M. Kozina, B. K. Ofori-Okai, S. P. Weathersby, S. Park, X. Shen, X. J. Wang, M. C. Hoffmann, R. K. Li, and E. A. Nanni, Femtosecond Compression Dynamics and Timing Jitter Suppression in a THz-Driven Electron Bunch Compressor, *Phys. Rev. Lett.* **124**, 054801 (2020).
- [29] L. R. Zhao, H. Tang, C. Lu, T. Jiang, P. F. Zhu, L. Hu, W. Song, H. D. Wang, J. Q. Qiu, C. G. Jing, S. Antipov, D. Xiang, and J. Zhang, Femtosecond Relativistic Electron Beam with Reduced Timing Jitter from THz Driven Beam Compression, *Phys. Rev. Lett.* **124**, 054802 (2020).
- [30] F. F. Qi, Z. R. Ma, L. R. Zhao, Y. Cheng, W. X. Jiang, C. Lu, T. Jiang, D. Qian, Z. Wang, W. T. Zhang, P. F. Zhu, X. Zou, W. S. Wan, D. Xiang, and J. Zhang, Breaking 50

- Femtosecond Resolution Barrier in MeV Ultrafast Electron Diffraction with a Double Bend Achromat Compressor, *Phys. Rev. Lett.* **124**, 134803 (2020).
- [31] H. W. Kim, N. A. Vinokurov, I. H. Baek, K. Y. Oang, M. H. Kim, Y. C. Kim, K. H. Jang, K. Lee, S. H. Park, S. Park, J. Shin, J. Kim, F. Rotermund, S. Cho, T. Feurer, and Y. U. Jeong, Towards jitter-free ultrafast electron diffraction technology, *Nat. Photonics* **14**, 245 (2020).
- [32] C. Varin, S. Payeur, V. Marceau, S. Fourmaux, A. April, B. Schmidt, P. L. Fortin, N. Thire, T. Brabec, F. Legare, J. C. Kieffer, and M. Piche, Direct electron acceleration with radially polarized laser beams, *Appl. Sci.* **3**, 70 (2013).
- [33] P.-L. Fortin, M. Piché, and C. Varin, Direct-field electron acceleration with ultrafast radially polarized laser beams: Scaling laws and optimization, *J. Phys. B: At. Mol. Opt. Phys.* **43**, 025401 (2009).
- [34] Y. I. Salamin, Electron acceleration from rest in vacuum by an axicon Gaussian laser beam, *Phys. Rev. A* **73**, 043402 (2006).
- [35] S. Carbajo, E. A. Nanni, L. J. Wong, G. Moriena, P. D. Keathley, G. Laurent, R. J. D. Miller, and F. X. Kartner, Direct longitudinal laser acceleration of electrons in free space, *Phys. Rev. Accel. Beams* **19**, 021303 (2016).
- [36] L. J. Wong and F. X. Kartner, Direct acceleration of an electron in infinite vacuum by a pulsed radially-polarized laser beam, *Opt. Express* **18**, 25035 (2010).
- [37] L. J. Wong and F. X. Kartner, Two-color-laser-driven direct electron acceleration in infinite vacuum, *Opt. Lett.* **36**, 957 (2011).
- [38] Z. Zhao, K. J. Leedle, D. S. Black, O. Solgaard, R. L. Byer, and S. Fan, Electron Pulse Compression with Optical Beat Note, *Phys. Rev. Lett.* **127**, 164802 (2021).
- [39] M. De Loos and S. Van Der Geer, in *5th European Particle Accelerator Conference (JACow, Barcelona, Spain, 1996)*, p. 1241.
- [40] S. Weathersby, G. Brown, M. Centurion, T. Chase, R. Coffee, J. Corbett, J. Eichner, J. Frisch, A. Fry, M. Gühr *et al.*, Mega-electron-volt ultrafast electron diffraction at SLAC national accelerator laboratory, *Rev. Sci. Instrum.* **86**, 073702 (2015).
- [41] T. Schietinger, M. Pedrozzi, M. Aiba, V. Arsov, S. Bettoni, B. Beutner, M. Calvi, P. Craievich, M. Dehler, F. Frei *et al.*, Commissioning experience and beam physics measurements at the SwissFEL injector test facility, *Phys. Rev. Accel. Beams* **19**, 100702 (2016).